Structure, Vol. 12, 215–226, February, 2004, ©2004 Elsevier Science Ltd. All rights reserved. DOI 10.1016/j.str.2004.01.005

Interactions of LY333531 and Other Bisindolyl Maleimide Inhibitors with PDK1

David Komander,[1,2] Gursant S. Kular,[2] Alexander W. Schüttelkopf,[1] Maria Deak,[2] K.R.C. Prakash,[4] Jennifer Bain,[3] Matthew Elliott,[3] Marta Garrido-Franco,[1,5] Alan P. Kozikowski,[4] Dario R. Alessi,[2] and Daan M.F. van Aalten[1,3,*]

[1]Division of Biological Chemistry and Molecular Microbiology
[2]MRC Protein Phosphorylation Unit
MSI/WTB Complex
School of Life Sciences
[3]Division of Signal Transduction Therapy
University of Dundee
Dundee DD1 5EH
Scotland
[4]Drug Discovery Program
Department of Neurology
Georgetown University Medical Center
Washington, DC 20007

Summary

LY333531, BIM-1, BIM-2, BIM-3, and BIM-8 are bisindolyl maleimide-based, nanomolar protein kinase C inhibitors. LY333531, a PKCβ-specific inhibitor, is in clinical trials against diabetes and cardiac ventricular hypertrophy complications. Specificity analysis with a panel of 29 protein kinases reveals that these bisindolyl maleimide inhibitors also inhibit PDK1, a key kinase from the insulin signaling pathway, albeit in the lower μM range. To understand the molecular basis of inhibition, the PDK1 kinase domain was cocrystallized with these bisindolyl maleimide inhibitors. The inhibitor complexes represent the first structural description of this class of compounds, revealing their unusual nonplanar conformation within the ATP binding site and also explaining the higher inhibitory potential of LY33331 compared to the BIM compounds toward PDK1. A combination of site-directed mutagenesis and essential dynamics analysis gives further insight into PDK1 and also PKC inhibition by these compounds, and may aid inhibitor design.

Introduction

3-phosphoinositide dependent protein kinase-1 (PDK1) plays a key role in insulin and growth factor signaling networks (Alessi, 2001). It phosphorylates and activates AGC (cAMP-dependent, cGMP-dependent, protein kinase C [PKC]) family kinases such as protein kinase B (PKB, also known as Akt) (Brazil and Hemmings, 2001), p70 ribosomal S6-kinase (S6K) (Avruch et al., 2001; Volarevic and Thomas, 2001), serum and glucocorticoid responsive kinase (SGK) (Lang and Cohen, 2001), p90 ribosomal S6 kinase (RSK) (Frodin and Gammeltoft, 1999), as well as isoforms of PKC (Newton, 2001, 2003). PKB, S6K, SGK, and certain isoforms of PKC are activated downstream of the second messenger phosphatidylinositol (3,4,5) trisphosphate [PtdIns(3,4,5)P_3] produced by phosphoinositide-3-kinase (PI 3-kinase) (reviewed in Leslie et al., 2001; Scheid and Woodgett, 2001). RSK isoforms are activated downstream of the classical ERK1/ERK2 signaling pathway (Frodin et al., 2000, 2002). In a significant number of cancers, mutations causing elevated levels of PtdIns(3,4,5)P_3 or ERK1/ERK2 occur, resulting in hyperactivation of AGC kinase family members, which is thought to contribute to the enhanced proliferation and survival of these cells. Because of this, there is considerable interest in developing inhibitors of PDK1 and other members of the AGC kinase family.

Much attention has been devoted to a group of bisindolyl maleimide compounds that are based on the scaffold of the nonspecific kinase inhibitor staurosporine (reviewed in Goekjian and Jirousek, 1999). These BIM compounds were originally reported to function as PKC selective inhibitors (Davis et al., 1992b), although subsequent work indicated that these were less specific than originally thought (Davies et al., 2000). A structurally related inhibitor termed LY333531 was also developed, which appeared to be more specific than other BIM compounds and inhibited the PKCβ isoform with two orders of magnitude higher potency than other PKC isoforms (Goekjian and Jirousek, 1999; Jirousek et al., 1996). Currently, LY333531 is in phase III clinical trials as a therapeutic agent for prevention of diabetes complications such as diabetic retinopathy (Nakamura et al., 1999), and also against left ventricular hypertrophy in heart failure, the latter probably due to effects on calcium sensitivity (Vlahos et al., 2003).

The BIM and LY333531 inhibitors chemically differ from staurosporine by the lack of a second covalent bond between the indole rings and by a change in the head group from a lactam to a maleimide moiety (Figures 1A–1F). These compounds are synthetically more accessible than staurosporine, and a large number of these derivatives have been synthesized (Figures 1B–1E) (Davis et al., 1992a, 1992b). Absence of the second bond linking the indole groups results in a nonplanar conformation, in contrast to the planar indolocarbazole derivatives such as staurosporine (Figures 1A–1E) (Davis et al., 1992b). LY333531 is similar to the BIM compounds, with an additional N12, N15-bridge linking the two indole rings without forcing them into a flat conformation (Figure 1A) (Jirousek et al., 1996).

In this study we describe and analyze the structures of the protein kinase domain of PDK1 bound to the bisindolyl maleimide inhibitors BIM-1 (also known as GF-109203X or Gö 6850; Toullec et al., 1991), BIM-2, BIM-3 (Fabre et al., 1993), BIM-8 (also known as Ro 31-7549; Ohtsuka and Zhou, 2002; Zhou et al., 1999), and LY333531 (Jirousek et al., 1996). These widely used inhibitors have not previously been crystallized with a protein kinase, and our results provide insight into their

*Correspondence: dava@davapc1.bioch.dundee.ac.uk
[5]Present address: Institute for Diabetes Research, Academic Hospital Schwabing, Kölner Platz 1, 80804 Munich, Germany.

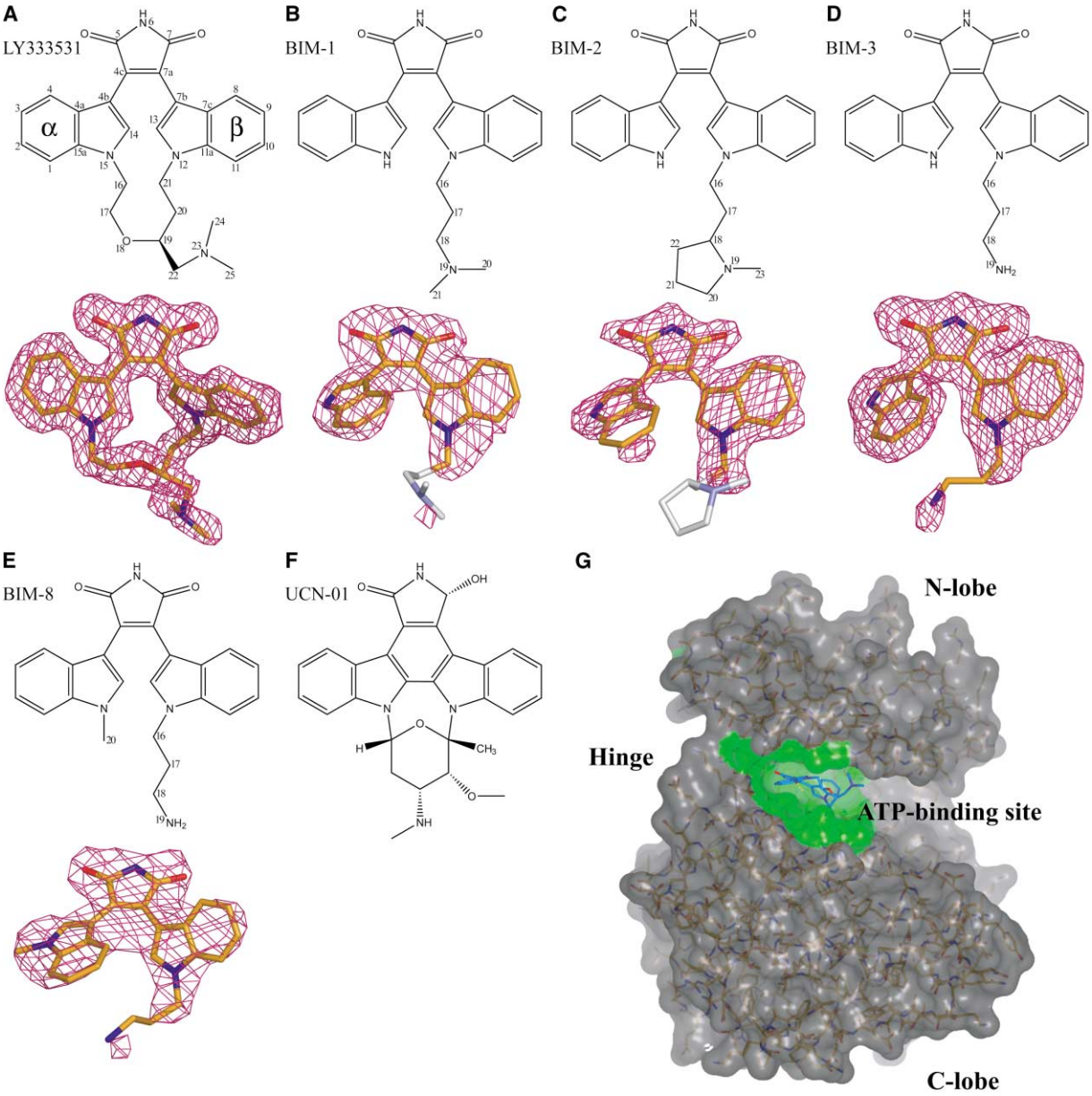

Figure 1. Two- and Three-Dimensional Representation of Bisindolyl Maleimides

(A–E) Two-dimensional representation of the kinase inhibitors used in this study, with numbering based on Takahashi et al. (1987). In addition, the three-dimensional structures of the inhibitors as seen in complex with PDK1 kinase domain are shown. The refined ligand models from the final refinement cycle are shown as stick representations with orange carbon atoms. Unbiased (i.e., before the ligand was included in the refinement) $|F_o|-|F_c|$, ϕ_{calc} maps are shown at 2.5 σ. Atoms from the flexible side chain of BIM-1 and BIM-2 that are not covered in electron density (gray carbon atoms) were refined with occupancy set to zero.

(F) Two-dimensional drawing of UCN-01, also termed 7-hydroxy-staurosporine.

(G) Overall representation of the PDK1 kinase domain in complex with LY333531. A stick model of PDK1 is covered with a gray, semitransparent surface. Residues of the ATP binding site are indicated by a green surface. The ligand is drawn as a stick representation with marine carbon atoms. The N- and C lobes, as well as the linker or hinge region, are labeled, respectively.

mechanism of action. We support the structural data with specificity analysis, site-directed mutagenesis of ATP binding site lining residues, and finally, essential dynamics analysis of the kinase-inhibitor complexes, the latter revealing a novel, inhibitor-induced conformational change.

Results and Discussion

Specificity of BIM and LY333531 Inhibitors

The specificities of LY333531, BIM-1, BIM-2, and BIM-8 were tested at a concentration of 10 μM against a panel of 29 protein kinases (Table 1). The specificity data for

Table 1. Specificity of LY333531, BIM-1, BIM-2, and BIM-8

Protein Kinase	LY333531 (10 μM)	BIM-1 (10 μM)	BIM-2 (10 μM)	BIM-8 (10 μM)
PKCα	0 ± 0	14 ± 1	2 ± 0	10 ± 1
PDK1	11 ± 3	43 ± 6	61 ± 4	14 ± 3
MSK1	13 ± 2	2 ± 1	3 ± 0	1 ± 1
MAPKAP-K1a	15 ± 15	1 ± 1	3 ± 3	21 ± 2
S6K1	19 ± 3	1 ± 4	26 ± 1	25 ± 7
Chk1	22 ± 1	13 ± 3	17 ± 1	5 ± 2
GSK3β	31 ± 2	8 ± 3	5 ± 3	6 ± 1
Phosphorylase kinase	35 ± 2	6 ± 1	7 ± 0	2 ± 1
AMPK	38 ± 7	5 ± 0	9 ± 0	2 ± 3
CDK2/cyclin A	39 ± 2	42 ± 8	25 ± 14	34 ± 3
PRAK	48 ± 0	90 ± 4	77 ± 3	66 ± 1
SGK	49 ± 1	16 ± 4	20 ± 4	15 ± 4
CSK	52 ± 2	88 ± 8	87 ± 9	87 ± 9
Lck	63 ± 4	28 ± 1	31 ± 2	23 ± 1
PKBΔph	67 ± 3	41 ± 1	46 ± 2	30 ± 1
MKK1	73 ± 9	71 ± 11	68 ± 5	35 ± 6
MAPKAP-K2	73 ± 5	36 ± 1	40 ± 5	16 ± 0
PKA	77 ± 7	41 ± 1	36 ± 4	22 ± 2
ROCK-II	79 ± 3	89 ± 12	82 ± 15	33 ± 0
SAPK2a/p38	87 ± 1	99 ± 3	86 ± 10	38 ± 11
DYRK1α	93 ± 4	3 ± 1	4 ± 1	2 ± 0
JNK/SAPK1c	96 ± 2	108 ± 11	104 ± 8	64 ± 1
CK1	96 ± 5	92 ± 0	84 ± 5	86 ± 9
NEK6	96 ± 6	61 ± 5	75 ± 8	21 ± 4
MAPK2/ERK2	98 ± 5	90 ± 3	90 ± 6	66 ± 7
SAPK2b/p38β2	98 ± 2	103 ± 11	82 ± 1	86 ± 4
CK2	100 ± 0	103 ± 11	89 ± 5	85 ± 1
SAPK3/p38γ	100 ± 3	101 ± 11	93 ± 7	75 ± 4
SAPK4/p38δ	104 ± 3	112 ± 5	92 ± 7	65 ± 8

The indicated protein kinases were assayed at 0.1 mM ATP as described previously (Bain et al., 2003; Davies et al., 2000) in the absence or presence of 10 μM inhibitor. Results are presented as percentage of kinase activity compared to that in control incubations. The activity results displayed in the two columns are an average of a triplicate determination. Abbreviations not defined in main text: MSK1, nuclear mitogen- and stress-activated protein kinase-1; MAPKAP, MAP kinase-activated protein kinase; GSK3β, glycogen synthase kinase 3β; CDK2, cyclin dependent protein kinase 2; SAPK, stress activated protein kinase; NEK6, NIMA (never in mitosis gene a)-related kinase 6; ROCK-II, Rho-dependent protein kinase-II; AMPK, AMP-activated protein kinase; MKK1, MAP-kinase kinase-1; PRAK, p38-regulated/activated protein kinase; CK2, Casein kinase-2; Chk1, cell cycle checkpoint kinase-1; DYRK, dual specificity tyrosine phosphorylated and regulated kinase; CSK, C-terminal Src kinase.

BIM-3 were reported previously (Davies et al., 2000). The results show that LY333531 is markedly more specific than the BIM inhibitors. At 10 μM LY333531, a high concentration of drug that completely abolishes PKCα activity, the activity of five other kinases was reduced to 15%–30%, with the remainder of the enzymes in the panel being inhibited to a lesser extent (Table 1). In contrast, in the presence of 10 μM BIM inhibitors, 6–7 kinases were inhibited by >90% and a further 4–10 inhibited by >70% (Table 1). Interestingly, we noticed that LY333531 and all of the BIM compounds inhibited PDK1 by around 40% (BIM-2) to 90% (LY333531) at 10 μM. The IC_{50} for PDK1 inhibition by LY333531 is 750 nM, for BIM-1 is 9 μM, for BIM-2 is 14 μM, for BIM-3 is 4 μM, and for BIM-8 is 1 μM.

Overall Structure of PDK1-Inhibitor Complexes

As the LY333531 and BIM inhibitors have not been crystallized with a kinase previously, we decided to cocrystallize the inhibitor molecules with the previously crystallized PDK1 catalytic domain (residues 51–359; Biondi et al., 2002). Diffraction data collection, structure solution by molecular replacement, and refinement resulted in the final models with statistics shown in Table 2. An overall picture of the PDK1 kinase domain is shown in Figure 1G, and initial $|F_o|-|F_c|$, ϕ_{calc} electron density for the ligands is shown in Figures 1A–1E.

LY333531 Bound to the PDK1 Kinase Domain

The PDK1-LY333531 complex at 1.70 Å represents the highest resolution PDK1 structure available to date. The overall structure of the catalytic domain of PDK1 complexed to LY333531 is shown in Figure 1G. In initial electron density maps, strong (>3 σ) $|F_o|-|F_c|$, ϕ_{calc} density could be observed in the ATP binding site, covering all atoms of LY333531 (Figure 1A). Within PDK1, LY333531 adopts a nonplanar conformation (Figure 1A) The α and β indole rings of LY333531 have torsion angles of 38° for the C4b-C4c torsion and of 30° for the C7a-C7b torsion, respectively (Figures 1A and 2). This results in a distance of 3.1 Å between the C13 and C14 carbon atoms. The linker between N12 and N15 displays an extended conformation, bridging a distance of 5.4 Å. LY333531 makes several contacts with the PDK1 kinase domain (Figure 2). The indole rings form hydrophobic interactions, with Leu88 (N lobe; see Figure 1G) and Gly165, Leu212 (C lobe) sandwiching the α indole ring, and Val96, Lys111 (N lobe), and Thr222, Asp223 (C lobe) packing against the β indole ring. In the recently reported structure of PDK1 in complex with staurosporine (Ko-

Table 2. Data Collection and Refinement Statistics

	PDK1-LY333531	PDK1-BIM-1	PDK1-BIM-2	PDK1-BIM-3	PDK1-BIM-8
Beamline	ID14-EH2	ID14-EH1	ID14-EH1	ID14-EH1	ID14-EH2
Wavelength (Å)	0.933	0.934	0.934	0.934	0.933
Space group	$P3_221$	$P3_221$	$P3_221$	$P3_221$	$P3_221$
Unit cell (Å)	$a,b = 121.62$	$a,b = 122.40$	$a,b = 121.95$	$a,b = 121.63$	$a,b = 123.68$
	$c = 47.875$	$c = 48.02$	$c = 48.07$	$c = 48.02$	$c = 47.79$
Resolution (Å)	25.0–1.70 (1.76–1.70)	25.0–2.50 (2.59–2.50)	25.0–1.90 (1.97–1.90)	25.0–1.95 (2.02–1.95)	25.0–2.80 (2.90–2.80)
Observed reflections	218856 (15901)	40461 (2832)	118992 (11353)	136516 (12803)	32999 (3180)
Unique reflections	44644 (4344)	13556 (1105)	32482 (3218)	29917 (2843)	9493 (915)
Redundancy	4.9 (3.7)	3.0 (2.6)	3.7 (3.5)	4.6 (4.4)	3.5 (3.5)
Completeness (%)	99.9 (98.6)	92.6 (75.6)	99.9 (99.8)	100 (100)	90.5 (90.3)
R_{merge}	0.044 (0.278)	0.089 (0.549)	0.076 (0.592)	0.100 (0.586)	0.138 (0.518)
$I/\sigma I$	22.1 (4.7)	9.8 (2.0)	10.0 (2.7)	6.9 (2.7)	8.5 (2.0)
Reflections in test set	665	547	670	623	521
R_{cryst}	0.176	0.199	0.240	0.183	0.193
R_{free}	0.204	0.259	0.279	0.224	0.245
Number of groups					
Protein residues	276	278	281	277	285
Water	283	47	180	227	81
Ligand atoms	35	31	33	29	30
SO_4^{2-} atoms	35	15	20	25	60
Glycerol atoms	54	42	24	48	20
Wilson B ($Å^2$)	19.6	53.3	22.2	20.7	50.2
<B> protein ($Å^2$)	18.9	41.3	23.5	23.5	28.9
<B> water ($Å^2$)	35.0	39.6	32.3	35.4	33.1
<B> ligand ($Å^2$)	14.5	50.5	25.0	19.6	29.5
Rmsd from ideal geometry					
Bond length (Å)	0.011	0.010	0.012	0.010	0.007
Bond angles (°)	1.45	1.72	1.43	1.73	1.66
Main chain *B* ($Å^2$)	0.86	1.49	0.73	1.44	1.38

Values between parentheses are for the highest resolution shell. All measured data were included in structure refinement.

mander et al., 2003), Val96 and Leu212 were identified as central hydrophobic residues contacting staurosporine from the N-terminal and C-terminal lobes, respectively. In the PDK1-LY333531 complex, due to the nonplanar nature of the ligand, these residues are 0.4 Å further apart than in the PDK1-staurosporine complex. The N12, N15 bridge of LY333531 spans the ATP binding site of PDK1 from the N lobe to the C lobe (Figure 2). C16 contacts the backbone of Leu88 and the Cα carbon of Gly89 in the phosphate positioning loop of the N lobe. Toward the C lobe, atoms C20 (Glu166, Glu209) and C21 (Glu209, Asn210) contact the linker region between the lobes (Figure 2). Electron density was also visible for the side chain extending from C19 (Figure 1A); however, this moiety is more disordered (<B> = 25.5 $Å^2$ compared to <B> = 13.0 $Å^2$ for the rest of the ligand) and is not involved in protein contacts. LY333531 makes three hydrogen bonds to the protein, from the maleimide portion of the molecule. The O5 carbonyl oxygen hydrogen bonds to the backbone nitrogen of Ala162, the imido group (N6) hydrogen bonds to the backbone carbonyl of Ser160, and the second carbonyl function at the seven-position (O7) hydrogen bonds to Oγ1 of Thr222 (Figure 2; Table 3). Interestingly, the first two hydrogen bonds mimic the interactions of the adenine base of ATP with PDK1, similar to all other kinase structures. Most ATP competitive inhibitors characterized to date also display equivalent hydrogen bonds to the kinase backbone (Hunenberger et al., 1999; Johnson et al., 1996). In contrast, the hydrogen bond from O7 to Thr222 is not conserved and this will be discussed in more detail below.

PDK1 in Complex with the Bisindolyl Maleimides 1, 2, 3, and 8

Four structures of PDK1 in complex with BIM compounds were determined. All structures showed $|F_o|-|F_c|$, ϕ_{calc} electron density in the ATP binding site, at a similar position as seen for LY333531 (Figures 1B–1E, and 2). The maleimide head group and the β indole ring of the four BIM compounds and LY333531 superimpose with an rmsd ≤0.3 Å. Therefore, the head groups show essentially the same hydrogen bonding pattern toward the protein backbone (Figure 2; Table 3). Remarkably, the β indole rings occupy the same space as the equivalent group in LY333531 (maximal shift 0.6 Å), contacting Leu159, Val96, Lys111, and Thr222. This implies that despite a different degree of rotational freedom of the indole rings of BIMs versus LY333531, the β indole ring adopts the same C7a-C7b torsion to fit the PDK1 ATP binding pocket. The α indole ring is seen at an equivalent position in all four BIM complex structures (maximal shift between equivalent atoms: 0.2 Å), but is flipped by 180° around the C4b-C4c bond compared to LY333531 (Figures 1A–1E, and 2). This arrangement of the indole rings is also found in the small molecule crystal structure for BIM-4 (Davis et al., 1992b), indicating that this conformation is energetically favorable. The different orientation of the α indole ring of the BIM compounds makes these molecules more compact (the largest distance between C2-C9 in LY333531 is 10.9 Å, compared to 8.6 Å between C9 and N15 in BIM-3) and less staurosporine-like compared to LY333531, resulting in fewer protein-ligand interactions. The carbonyl oxygen of

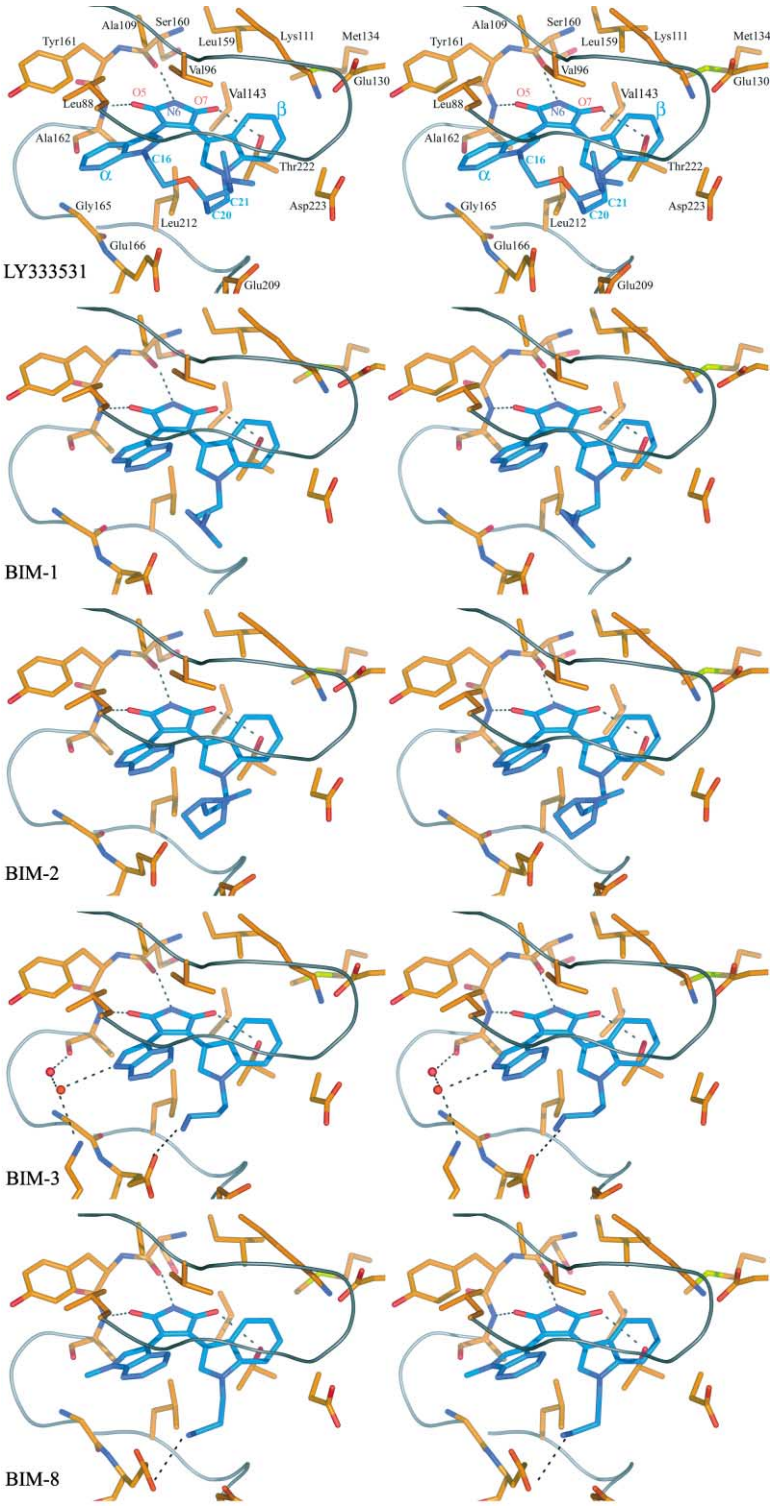

Figure 2. Stereo Representation of Ligand Interactions within the ATP Binding Pocket of PDK1

Ligand carbon atoms are colored in marine, and protein carbon atoms are in orange. Water molecules are shown as purple spheres. Hydrogen bonds are indicated by black dotted lines. A gray ribbon indicates the protein backbone.

Ala162 (in LY333531, distance 3.4 Å from C3) is now 4.4 Å away from C14 of BIM-3 and therefore does not interact with the ligand (Figure 2). The distance between Cα of Gly165 and the ligand increases from 3.5 Å (to C3 of LY333531) to 4.8 Å (to N15 of BIM-3), creating a void between the α indole ring and the linker region connecting the two kinase lobes. Although the α indole ring is flipped in the BIM compounds, it maintains similar stacking interactions to those observed for LY333531, between Leu88 and Leu212. The α indole nitrogen N15 in the BIM compounds points toward the solvent-accessible side of the ATP binding pocket. In BIM-3, two ordered water molecules (B factors = 34.4 Å^2, 43.3 Å^2) are found between the linker region and the ligand, cre-

Table 3. IC_{50} Values and Hydrogen Bonding Potential of Maleimides and UCN-01 in Complex with PDK1

	LY333531	BIM-1	BIM-2	BIM-3	BIM-8	UCN-01
IC_{50} (μM)	0.75	9	14	4	1	0.006
Ligand O5-Ala162 N						
d_{DA} (Å)	3.1	3.1	3.1	3.0	3.1	2.8
HB2	0.7	0.5	0.5	0.7	0.5	0.8
Ligand N6-Ser160 O						
d_{DA} (Å)	2.9	3.0	2.7	2.9	3.0	2.9
HB2	0.6	0.6	0.6	0.6	0.6	0.8
Ligand O7-Thr222 Oγ1						
d_{DA} (Å)	3.0	3.0	3.1	3.0	3.0	3.0
HB2	0.7	0.6	0.6	0.6	0.7	0.6
Ligand N19-Glu166 Oϵ2						
d_{DA} (Å)				3.0	2.7	
HB2				0.5	0.5	

Hydrogen bonds between inhibitors and PDK1 were calculated with WHAT IF (Vriend, 1990) using the HB2 algorithm (Hooft et al., 1996). This algorithm gives a score between 0 (no hydrogen bond) and 1 (optimal hydrogen bond) to reflect hydrogen bond geometry (HB2 row). Donor-acceptor distances (d_{DA}) are also listed.

ating a hydrogen bonding network and contacting N15 of BIM-3 (3.3 Å), the backbone carbonyl of Ala162 (2.9 Å), and also Nζ of Lys169 (3.1 Å) (Figure 2). In contrast, no water molecules could be observed at equivalent positions for BIM-1 or BIM-2 in complex with PDK1 (Figure 2). In BIM-8, the N15 nitrogen possesses a methyl group. The variable side chains attached to N13 of the β indole ring distinguish the BIM inhibitors from each other (Figures 1B–1E). These side chains are structurally less ordered in complex with PDK1, as indicated by higher B-factors compared to the rest of the molecule (e.g., for BIM-3: $<B>_{core} = 18.0$ Å^2 versus $<B>_{side\ chain} = 29.9$ Å^2), as well as weak density for some atoms (Figures 1B–1E).

Correlation of IC_{50} with Hydrogen Bonding

The hydrogen bonding of LY333531 and the BIM inhibitors with the PDK1 kinase domain was assessed using the HB2 algorithm (Table 3) (Hooft et al., 1996). All inhibitors display three hydrogen bonds from the polar groups of their maleimide moieties (O5-Ala162, N6-Ser160, and O7-Thr222), which appear to have equal strength (Table 3). As discussed above, two of these interactions are highly conserved and also visible in the binding mode of the adenine base in ATP (Biondi et al., 2002), as well as with staurosporine and UCN-01 binding (Komander et al., 2003). However, in the present structures both of these hydrogen bonds have poorer geometry for both LY333531 and the BIM compounds compared to UCN-01 (Table 3). The third maleimide hydrogen bond from O7 to Thr222-Oγ1 is also found in the complex of PDK1 with UCN-01, which possesses a hydroxy group instead of a second carbonyl group at the C7 position (Figure 1F). In the maleimide inhibitors, this hydrogen bond displays similar geometry than observed for UCN-01 (Table 3). As mentioned above, different IC_{50} values are found for LY333531 and BIM inhibitors, with 0.75 μM (LY333531), 1 μM (BIM-8), 4 μM (BIM-3), 10 μM (BIM-1), and 14 μM (BIM-2) (Table 3). BIM-3 and BIM-8 possess an additional fourth hydrogen bond from the terminal side chain amino group (N19) to the Oϵ2 of Glu166 (Figure 2). It can be noted that the additional hydrogen bond correlates with a 3- to 10-fold lower IC_{50} compared to BIM-1 and BIM-2, which lack a side chain capable of hydrogen bonding (Figures 1B–1E; Table 3). Additionally, the terminal amino group in BIM-3 and BIM-8 is likely to provide electrostatic interactions with the protein, and such interactions have been noted to be beneficial for ligand binding in PKA (Hunenberger et al., 1999). This observation could be used in future inhibitor design. However, LY333531 does not possess this extra hydrogen bond, yet it is the only inhibitor with an IC_{50} below 1 μM. A possible explanation for this could be the contribution of entropic effects on ligand binding. The indole rings (Figures 1B–1E) in the BIM compounds would be expected to have considerable rotational freedom in solution, yet are tethered in the PDK1 complexes. In LY333531, however, the indole rings are not free to rotate due to the presence of the additional N12, N15 bridge (Figure 1A), and consequently, a lower entropic penalty would have to be paid upon binding to PDK1. Measurement of such potential entropic effects by isothermal titration microcalorimetry was not successful due to weak solubility of the ligands.

Comparison of LY333531 and UCN-01 Binding to PDK1

Compared to UCN-01 inhibition ($IC_{50} = 0.006$ μM), the inhibitors described here show a 100- to 2000-fold higher IC_{50} against PDK1. Apart from the weaker hydrogen bonds (Table 3), and the described putative entropic effects, it is possible that there are other features of the staurosporine scaffold which contribute to its greater inhibitory potential. As the most staurosporine-like inhibitor, LY333531, is the most potent inhibitor with an IC_{50} below 1 μM, we compared the complexes of PDK1-LY333531 and PDK1-UCN-01. As mentioned above, UCN-01 possesses a lactam head group and a 7-hydroxy group, rather than a maleimide 7-carbonyl. The change from a planar carbonyl C7 in LY333531 to a tetragonal C7 in UCN-01 places the hydroxy group out of the aromatic plane, toward the C lobe, where it makes a hydrogen bond to Thr222 (Figures 1A and 1F; Table 3) (Komander et al., 2003). However, superposition of both protein structures (rmsd on main chain atoms: 0.42 Å) shows that the head groups of both ligands do not superim-

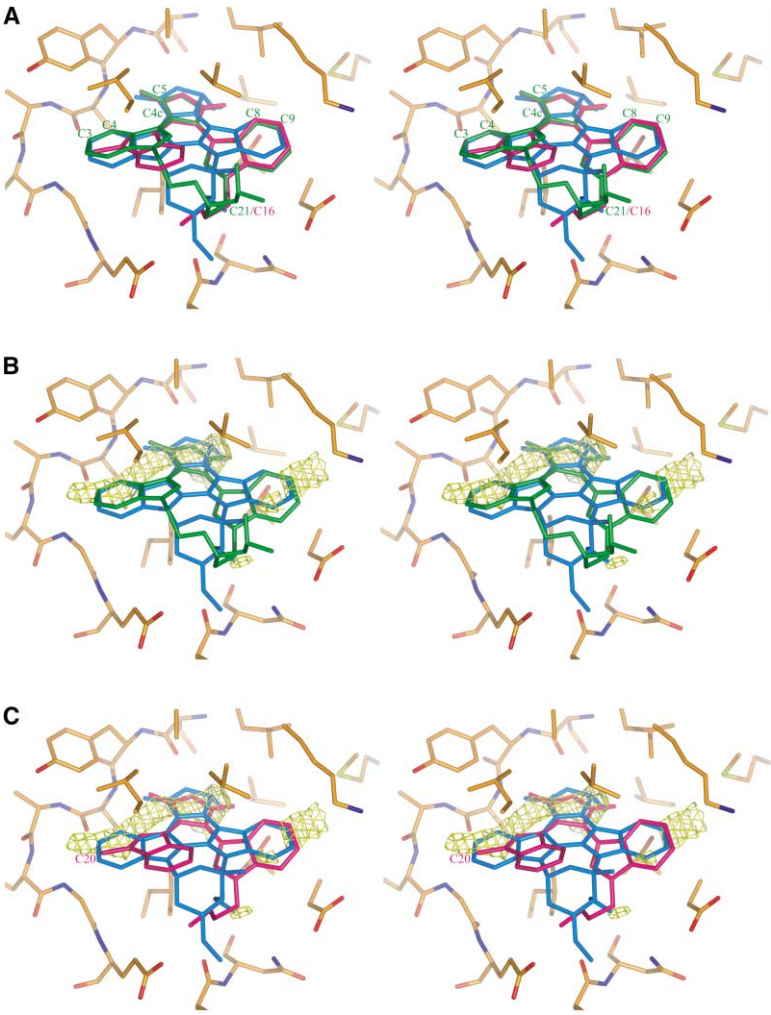

Figure 3. Conserved Carbon Positions in the PDK1 ATP Binding Site

(A) Superposition of LY333531 (dark green) and BIM-8 (magenta) bound to the PDK1-UCN-01 complex (with PDK1 colored as in Figure 2, and UCN-01 colored in marine). The rotation of the maleimide head group as well as conserved carbon positions within the staurosporine scaffold are visible, with atoms numbered as in Figure 1A.

(B) A carbon affinity grid (in yellow) shows the preferred positions of carbon atoms within the ATP binding site of the PDK1-UCN-01 complex. The grid is contoured at a binding potential energy of −0.55 kcal/mol and is located around conserved carbon positions for UCN-01 (marine) and LY333531 (dark green).

(C) The same grid as in (B), with BIM-8 (magenta) superimposed onto UCN-01 (marine).

pose, but display a tilt of approximately 20° along the C4c-C5 axis of the maleimide compared to UCN-01 (Figure 3A). This results in a shift of the LY333531 O5 oxygen of 0.5 Å toward the N lobe and in a shift of the N6 atom of 0.3 Å in the other direction. The largest distance between equivalent atoms of the five-membered rings is 0.6 Å for the C7 carbon. However, as a result of this different orientation, the 7-hydroxy group of UCN-01 and the 7-carbonyl oxygen of LY333531 are positioned to within 0.5 Å. The rotation therefore enables the O7 of LY333531 to hydrogen bond Oγ1 of Thr222 (Figure 3A; Table 3), but at the same time weakens the remaining hydrogen bonds (Table 3). As mentioned above, the maleimide head groups of the BIM compounds superimpose with that of LY333531, and therefore these are also tilted compared to UCN-01 (Figures 3A and 3C). However, such rotation of the maleimide head group is not observed in the only other maleimide inhibitor protein kinase complex described to date. Structures of the cell cycle checkpoint kinase Chk1 have been reported in complex with UCN-01 and the staurosporine analog SB218078, which contains a maleimide head group (PDB codes 1NVQ, 1NVS) (Zhao et al., 2002). Both ligands inhibit Chk1, with apparent K_i's of 5.6 nM (UCN-01) and 15 nM (SB218078), respectively (Zhao et al., 2002). Chk1 binds the 7-hydroxy group of UCN-01 with Ser147-Oγ (equivalent to Thr222) (Komander et al., 2003; Zhao et al., 2002). However, no direct hydrogen bond can be observed between Ser147-Oγ and the 7-carbonyl oxygen of SB218078 (distance 4.4 Å). Thus, SB218078 does not orient itself to form a third hydrogen bond, as observed for complexes of PDK1 with maleimides. This indicates that in Chk1, the hydrophobic interactions of the ligand with the kinase are more important than the formation of an additional hydrogen bond, and this finding is consistent with theoretical models (Hunenberger et al., 1999).

Identification of Conserved Carbon Positions in the PDK1 ATP Binding Site

It is surprising that although the maleimide head group is rotated and the indole rings are tilted compared to UCN-01, two aromatic C-C bonds of UCN-01 within the indole rings closely overlap with the LY333531 indole rings (Figure 3A). The bonds between C3 and C4 and between C8 and C9 are shifted less than 0.15 Å in the superimposed PDK1-UCN-01 and PDK1-LY333531 complexes, whereas other equivalent atoms shift up to 0.7 Å in the α indole ring and up to 1.9 Å in the β indole ring (Figure 3A). This finding suggests that despite over-

all differences in ligand orientation, the position of certain atoms is fixed within the ligand binding site. To assess this on a more quantitative scale, the structure of PDK1 in complex with UCN-01 was used to generate an affinity grid for a carbon probe with AUTODOCK3 (Morris et al., 1998). This grid determines the energy of interaction between isolated carbon atoms and the PDK1 ATP binding site. Consistent with the observed superposition of particular carbon atoms at the C3-C4 and C9 positions, local minima were observed with binding energies of approximately −0.55 kcal/mol (Figures 3B and 3C). Interestingly, an additional local minimum is observed around the ether carbon of the sugar moiety of UCN-01, which superimposes with C21 of the N12, N15 bridge of LY333531, and also with C16 of the flexible side chain of BIM compounds (Figures 3B and 3C). A comparison with grids calculated for other probe atoms showed that carbon has the highest affinity to these positions (data not shown). This suggests a preference of PDK1 for carbon atoms at these particular positions, which is satisfied by both staurosporine derivatives and LY333531, but only partially (for the C9 and the C16 position) by the BIM compounds. Due to the flipped α indole ring, the BIM inhibitors do not occupy the favorable carbon positions equivalent to C3-C4 in LY333531, making these compounds less staurosporine-like (Figures 2 and 3). Interestingly, the most potent BIM inhibitor, BIM-8, possesses a methyl group (C20) (Figures 1E, 3A and 3C) on N15, which occupies a position within 1.1 Å of C3 in LY333531/UCN-01 (Figures 3A and 3C) and therefore might account for increased affinity of the inhibitor. Whether the observed rotation of the maleimide head group occurs to satisfy a third hydrogen bond, or to maximize hydrophobic interactions, can only be speculated. The theoretical description of ligand binding determinants for PKA (Hunenberger et al., 1999) seems to support the latter possibility.

LY333531 Inhibition of PKCβ-like PDK1 Mutants

As LY333531 is assumed to be a selective PKCβ inhibitor, but no structural data for any PKC isoform is available to date, the basis for the selectivity and potency of LY333531 for PKCβ is unknown. In an attempt to understand why, compared to PDK1, PKCβ is inhibited two orders of magnitude more potently by LY333531, the key residues in PDK1 which contact LY333531 and differ in PKCβ (Val143, Leu159, Ala162, Glu166, and Thr222) were mutated in PDK1 to their PKCβ equivalents. The mutants generated were PDK1[Val143Thr], PDK1[Leu159Met], PDK1[Ala162Val], PDK1[Glu166Asp], PDK1[Thr222Ala], and the double mutant PDK1[Val143Thr, Thr222Ala]. These mutants possessed similar specific activity toward the PDK1 peptide substrate as wild-type PDK1, and the IC_{50} for LY333531 and BIM-3 for the mutants was determined (Table 4). The only mutation that marginally decreased the IC_{50} (from 750 nM to 500 nM for LY333531 inhibition and from 3.8 to 2.5 μM for BIM-3 inhibition) was PDK1[Val143Thr]. From analyzing the PDK1-LY333531 structure, it appears that exchange of Val143 to Thr could enable PDK1 to hydrogen bond the O7 oxygen of the maleimide head group with better geometry. We therefore propose that this interaction in PKC isoforms could be more beneficial for the geometry of the remaining, conserved hydrogen bonds. BIM-3 and BIM-8 make an additional, fourth hydrogen bond toward Glu166 in PDK1. In the PDK1[Glu166Asp] mutant, the IC_{50} increases marginally (from 3.8 to 5.7 μM), indicating a potential positive contribution of this residue to ligand binding. As discussed above, in wild-type PDK1, Thr222 hydrogen bonds to O7 of LY333531 (Figure 2; Table 3). However, the finding that both wild-type PDK1 and the PDK1[Thr222Ala] mutant were similarly inhibited by LY333531 indicates that this interaction does not contribute significantly to LY333531 binding to PDK1, and this was also observed for the binding of UCN-01 to PDK1 (Komander et al., 2003). The remaining mutations would be anticipated to change the shape and volume of the ATP binding pocket, but none were found to significantly influence the ability of PDK1 to be inhibited by either LY333531 or BIM-3 (Table 4). We interpret these results as implying that the overall shape of the ATP binding site, rather than one specific residue, is responsible for the high-affinity binding of LY333531 to PKCβ compared to PDK1. This contrasts with other kinase inhibitors, such as the pyridinylimidazole SB203580 p38 MAP kinase inhibitor, where the presence of a small amino acid residue (Thr106 in p38α) at a position occupied by large amino acid residue in most other kinases (e.g., Leu159 in PDK1), accounts for the specific inhibition of these enzymes by SB203580 (Eyers et al., 1998, 1999). However, we can of course not exclude that the shape of the PKCβ ATP pocket possesses other features that account for the high-affinity binding to LY333531.

Another striking fact is the isoform specificity of LY333531 toward PKCβ. PKCα, which differs from PKCβ by 6 nonconservative and 20 conservative mutations within the kinase domain (all of which are remote from the ATP binding site in a PKCβ model based on our complex structure), is inhibited with an order of magnitude lower potency. All predicted residues contacting the ligand would be identical between the α- and β isoforms of PKC and are unlikely to account for the difference in inhibition. Therefore, other factors have to contribute to the isoform specificity of LY333531, and detailed (structural) analysis of PKC isoforms will be necessary to identify these factors. For instance, the conformational state of the kinase domain could be a contributing factor to inhibitor potency, as will be discussed in the following section.

Essential Dynamics Calculation on Available PDK1 Structures

Analyses of protein kinase A (PKA) structures have highlighted the conformational flexibilities of protein kinases (Biondi et al., 2002; Johnson et al., 2001). The two lobes of the kinase domain are connected via a hinge (Figure 1G), which accounts for the mobility of the kinase lobes relative to each other. For PKA, active, "closed" conformations and inactive, "open" conformations have been described (Johnson et al., 2001). Certain inhibitors, such as staurosporine or balanol, bind to the PKA kinase domain, locking it in an "intermediate" conformation (Narayana et al., 1999; Prade et al., 1997). Therefore, it may be necessary to study ligand-induced conforma-

Table 4. IC_{50}s of LY333531 Inhibition for PDK1 Mutants

PDK1 mutant	Specific Activity (U/mg)	IC_{50} LY333531	IC_{50} BIM-3
Wild type PDK1	158	750 nM	3.8 μM
PDK1[Val143Thr]	153	500 nM	2.5 μM
PDK1[Leu159Met]	147	600 nM	3.0 μM
PDK1[Ala162Val]	156	743 nM	3.4 μM
PDK1[Glu166Asp]	86	610 nM	5.7 μM
PDK1[Thr222Ala]	157	734 nM	3.8 μM
PDK1[Val143Thr/Thr222Ala]	180	500 nM	2.0 μM

tional changes in protein kinases and design methods that include such information in the inhibitor design process.

Compared to the recently reported structure of PDK1 in complex with staurosporine (Komander et al., 2003), two central hydrophobic residues (Val96 and Leu212) are shifted by 0.4 Å upon binding of BIM inhibitors, which may have an effect on the overall conformation of PDK1. To investigate this, the overall conformational state of PDK1 was analyzed using an essential dynamics approach. This technique extracts large concerted motions from an ensemble of structures (Amadei et al., 1993) and has previously been applied to collections of crystal structures (Biondi et al., 2002; de Groot et al., 1998; van Aalten et al., 1997, 2000). To assess the effect of different ligands on the overall conformation of the PDK1 kinase domain, we used structures of PDK1 in complex with ATP (PDB id 1H1W) (Biondi et al., 2002), staurosporine (1OKY), UCN-01 (1OKZ) (Komander et al., 2003), LY333531, BIM-1, BIM-2, BIM-3, BIM-8 (all this study), and unpublished structures of PDK1 with MgAMPPNP, HisPDK1 (histidine-tagged PDK1) with MgADP, and PDK1 with a partially occupied ATP binding site. All crystals were obtained under similar conditions and had the same space group and similar unit cell dimensions. Using EDprep (A.W.S., unpublished data), the backbone atoms of the common core of the PDK1 structures were extracted. From the resulting models, comprising residues 74–230 and 244–357, a covariance matrix was generated. Diagonalisation of this matrix yielded a set of eigenvectors/eigenvalues describing the concerted shifts of atoms. The projection of the PDK1 structures onto the subspace spanned by the first two eigenvectors, which describe a hinge-bending motion and a twisting motion, respectively, is shown in Figure 4. A similar analysis of the concerted motions of available PKA structures (Biondi et al., 2002) showed that the first two eigenvectors were found to describe qualitatively similar motions (hinge bending and twisting), but the magnitude of these motions seems to be significantly greater for PKA than for PDK1. This might reflect a higher intrinsic flexibility of PKA, but it cannot be excluded that experimental factors such as crystal packing might contribute to the limited flexibility observed for PDK1.

The hinge bending, visualized by the first eigenvector, has also been described for other protein kinases, such as PKA (Johnson et al., 2001) and CDK2 (Jeffrey et al., 1995), and results in their open (inactive) and closed (active) conformations (Figure 4). The structures of PDK1 are distributed along the first eigenvector, indicating different degrees of opening. PDK1 in complex with staurosporine and UCN-01 display the most closed conformations of PDK1. The bisindolyl maleimides described in this study induce open conformations of PDK1. The most open of the present PDK1 structures is the complex with BIM-2, followed by BIM-3, BIM-1, and LY333531. The second eigenvector describes a twisting motion between the N-terminal and the C-terminal lobe. Interestingly, all PDK1-inhibitor complexes appear in a different "twist state" compared to the structures with PDK1's natural ligand ATP (Figure 4). This novel finding highlights the contribution of inhibitor binding to overall protein conformation.

Conclusions

We have described the structures of the kinase domain of PDK1 in complex with the bisindolyl maleimide-based inhibitors LY333531, BIM-1, BIM-2, BIM-3, and BIM-8. Apart from LY333531, which shows significant selectivity for PKC isoforms, bisindolyl maleimide inhibitors are not specific. Due to the lack of a second covalent linkage of the indole rings compared to indolocarbazoles such as staurosporine, all ligands adopt a nonplanar conformation in the ATP binding site of PDK1. This nonplanar conformation, however, is different between the BIMs and LY333531 due to the N12, N15 bridge of the latter. We identified five effects that could contribute to ligand affinity. First, the quality of conserved hydrogen bonds seems to be correlated inhibitory potential. This was deduced from the fact that a tilt in the maleimide head group by 20° enables a third hydrogen bond from the ligand O7, but at the same time significantly affects the geometry of the remaining, conserved hydrogen bonds. Second, addition of a side chain with a terminal amino group makes an additional hydrogen bond which mimics the contact to the sugar moiety in both the ATP (Biondi et al., 2002) and the staurosporine complexes (Komander et al., 2003) and has a positive effect on inhibition. Third, the chemical structure of the ligand contributes to affinity, as BIM compounds have a higher degree of rotational freedom compared to LY333531 and staurosporine, and therefore a higher entropic penalty is to be paid upon fixing these molecules in the ATP binding site of PDK1. Fourth, preferred positions for carbon atoms within the ATP binding site of PDK1 were identified, and the occupation of these sites is correlated with the inhibitory potential. Finally, we provide evidence that the overall protein conformation is also likely to play a key role in inhibitor binding and specificity. Although the bisindolyl maleimide inhibitors are neither specific nor particularly good inhibitors of PDK1, their structures in complex with PDK1 have lead to new insights into PDK1 ligand binding with a novel class of inhibitors. Our find-

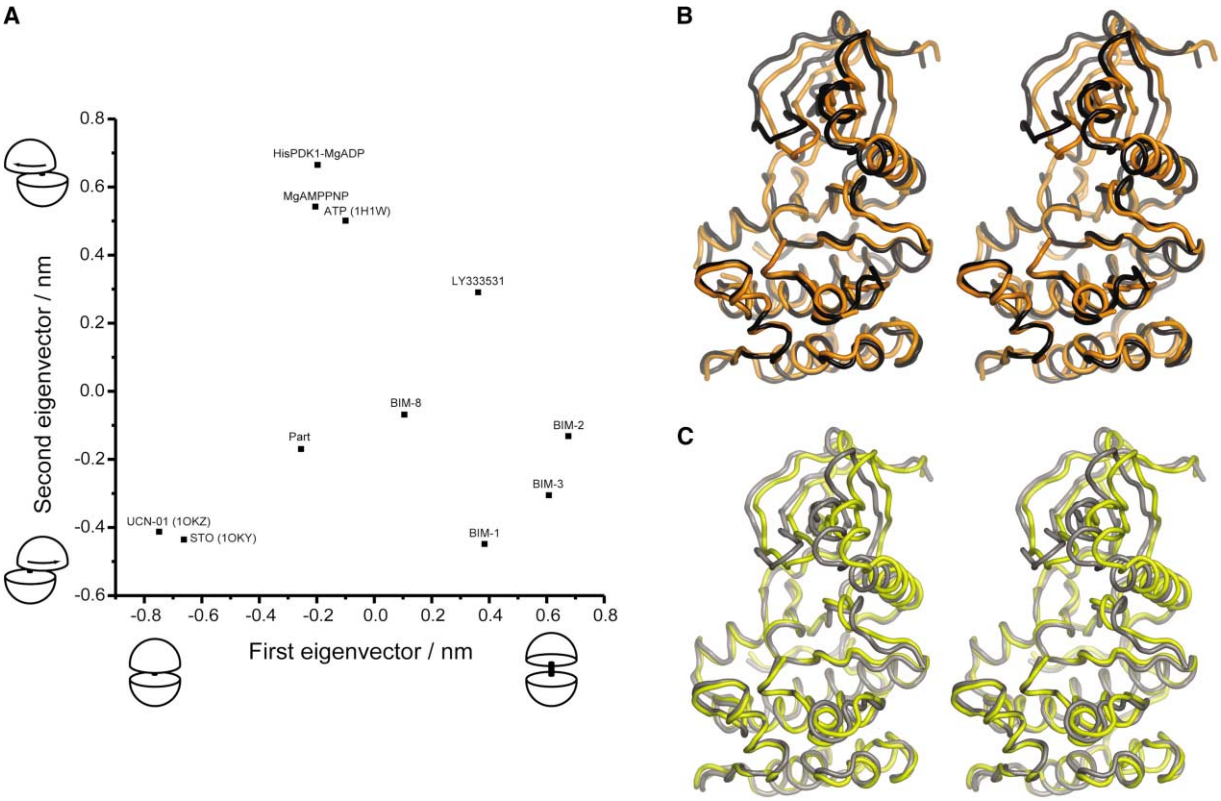

Figure 4. Essential Dynamics Analysis of PDK1 Structures

(A) Projection of analyzed PDK1 crystal structures (labeled squares) onto the first eigenvector, describing the hinge-bending motion, and the second eigenvector, describing the twisting motion, calculated from the PDK1 structures. The first two eigenvectors describe approximately 60% of the motions derived from PDK1 kinase structures. Abbreviations not explained in the text are STO (staurosporine) and Part (PDK1 with a partially occupied ATP binding site).

(B and C) Visualization of the motion described by the first (B) and second (C) eigenvector. The structures projected at −2 nm and +2 nm total atomic displacements along the respective eigenvectors are shown, superimposed on the C lobe.

ings could be useful for the design of new PDK1 inhibitors. Apparently a 7-hydroxy group (as in UCN-01) instead of a 7-carbonyl group (as in maleimides) may improve the alignment of the remaining hydrogen bonds.

Experimental Procedures

Protein Expression, Purification, and Crystallization

PDK1 (residues 51–359) was expressed in insect cells (SF21) and purified as described previously (Biondi et al., 2002; Komander et al., 2003). The protein was concentrated to 2 mg/ml (determined by Bradford assay with BSA as a standard), mixed with 10% glycerol, and frozen at −80°C. Prior to crystallization, the glycerol was diluted out with buffer A (500 mM NaCl, 25 mM Tris [pH 7.5]) during the concentration process. 3 ml PDK1 at a concentration of 0.5 mg/ml was mixed with 15 μl LY333531 (10 mM in DMSO), incubated on ice for 2 hr, and concentrated to 7.3 mg/ml. Dark purple, rod shaped crystals were grown from 2.1 M ammonium sulfate, 0.1 M Tris-HCl [pH 8.0], 10% (v/v) phenol using the vapor diffusion approach in a sitting drop setup and reached a maximal size of 0.2 × 0.2 × 0.5 after 5 days. BIM-2 (45 μl, 10 mM in 50% ethanol) and BIM-3 (30 μl, 10 mM in water) were preincubated with PDK1 (1.5 ml of 2 mg/ml solution each) and subsequently concentrated to 5.8 and 6.1 mg/ml, respectively. Orange, rod-shaped crystals appeared in 2.3 M ammonium sulfate, 0.1 M Tris-HCl [pH 8.25] for PDK1-BIM-2 and in 2.2 M ammonium sulfate, 0.1 M Tris-HCl [pH 8.25] for PDK1-BIM-3 in a sitting drop setup. BIM-1 and BIM-8 were cocrystallized with PDK1 by adding 10 μl BIM-1 (10 mM in ethanol) to 100 μl PDK1 at 6.6 mg/ml or 5 μl BIM-8 (50 mM in 30% ethanol) to 50 μl of PDK1 at 8.5 mg/ml. Crystals of PDK1-BIM-1 grew as orange rods from 2.1 M ammonium sulfate, 0.1 M Tris-HCl (pH 7.5), and crystals of PDK1-BIM-8 grew as brown stars of thin rods from 2.0 M ammonium sulfate, 0.1 M Tris-HCl (pH 7.75). Prior to data collection, crystals were soaked in a cryoprotectant containing 1.7 M ammonium sulfate, 0.1 M Tris [pH 7.5], 20% (v/v) glycerol for 5 s and frozen in a nitrogen cryo stream.

Data Collection and Structure Determination

Data on PDK1-inhibitor complexes were collected at the ESRF beam-lines ID14-EH1 and ID14-EH2 (Table 1), using an ADSC Q4 CCD detector. The temperature of the crystals was maintained at 100 K using a nitrogen cryostream during the data collection. Data were processed using the HKL package (Otwinowski and Minor, 1997), with final statistics shown in Table 1. All datasets displayed the space group $P3_221$ with one molecule per asymmetric unit and were processed to 1.70 Å (LY333531), 2.50 Å (BIM-1), 1.90 Å (BIM-2), 1.95 Å (BIM-3), and 2.80 Å (BIM-8). The structure of PDK1 with LY333531 was solved by molecular replacement with AMoRe (Navaza, 2001) using the PDK1-ATP complex (PDB id 1H1W) (Biondi et al., 2002) as a search model, with an initial R factor of 28.1% (R_{free}, 30.1%). Refinement of the PDK1-BIM complexes was initiated by rigid body refinement in CNS (Brunger et al., 1998) using the PDK1-ATP complex as a starting model. Initial R factors ranged from 27.5% (R_{free} = 27.2%) for the PDK1-BIM-8 complex to 33.2% (R_{free} = 35.4%) for the complex of PDK1 bound to BIM-3. Simulated annealing in CNS was used in the first rounds of refinement to reduce model bias, and sequential rounds of model building in O (Jones et al., 1991) and refinement using CNS were performed. Final

rounds of refinement for PDK1-LY333531 and PDK1-BIM-2 were performed in REFMAC5 (Murshudov et al., 1997). Strong ($>3.0\ \sigma$) electron density in the ATP binding pocket was observed for all inhibitor molecules in the unbiased $|F_o|-|F_c|$, ϕ_{calc} maps (Figures 1A–1E). After initial rounds of model building, the inhibitor molecules were included in refinement, using topology and parameter files generated by PRODRG (van Aalten et al., 1996). Furthermore, electron density for glycerol molecules, sulfate ions, and water molecules could be observed, and these were included in the final models, resulting in the final refinement statistics as shown in Table 2.

Mutational Analysis, Determination of Inhibition, and Specificity

The mutants PDK1[Val143Thr], PDK1[Leu159Met], PDK1[Ala162Val], PDK1[Glu166Asp], PDK1[Thr222Ala], and the double mutant PDK1[Val143Thr, Thr222Ala] were generated using site-directed mutagenesis with the QuikChange mutagenesis kit (Stratagene) in the pEBG2T vector. PDK1 and the indicated mutants were expressed as glutathione-S-transferase (GST) fusion proteins in 293 cells and purified as described previously (Biondi et al., 2002). Wild-type PDK1 (Alessi et al., 1997) was assayed for 10 min at 30°C in a 50 μl assay mixture in 50 mM Tris (pH 7.5), 0.1 mM EGTA, 0.1% 2-mercaptoethanol, containing 100 μM substrate peptide (PDK1tide, KTFCGTPEYLAPEVRREPRILSEEEQEMFRDFDYIADWC), 10 mM magnesium acetate, 100 μM [γ-^{32}P]ATP (200 cpm/pmol) as described previously (Biondi et al., 2000). Other protein kinases employed in Table 1 were assayed as described previously (Bain et al., 2003; Davies et al., 2000).

Chemistry of the BIMs

LY333531 was synthesized according to published procedures (Faul et al., 1998; Jirousek et al., 1995, 1996). BIM-1, BIM-2, BIM-3, and BIM-8 were synthesized according to the procedures published in Davis et al. (1992a) and Xie and Lown (1994).

All figures were created with PyMol (www.pymol.org).

Acknowledgments

We would like to thank the European Synchrotron Radiation Facility for beam time at ID14-EH1 and ID14-EH2. D.K. is funded by an MRC Predoctoral Fellowship, M.G.F. was supported by an EMBO long-term fellowship (ALTF 752-2002), and D.M.F.v.A. is supported by a Wellcome Trust Career Development Research Fellowship. D.R.A. thanks the Association for International Cancer Research, Diabetes UK, the Medical Research Council, and the pharmaceutical companies AstraZeneca, Boehringer Ingelheim, GlaxoSmithKline, Novo-Nordisk, and Pfizer for supporting the Division of Signal Transduction Therapy unit in Dundee.

Received: September 16, 2003
Revised: October 20, 2003
Accepted: October 21, 2003
Published: February 10, 2004

References

Alessi, D.R. (2001). Discovery of PDK1, one of the missing links in insulin signal transduction. Colworth Medal Lecture. Biochem. Soc. Trans. *29*, 1–14.

Alessi, D.R., James, S.R., Downes, C.P., Holmes, A.B., Gaffney, P.R., Reese, C.B., and Cohen, P. (1997). Characterization of a 3-phosphoinositide-dependent protein kinase which phosphorylates and activates protein kinase Balpha. Curr. Biol. *7*, 261–269.

Amadei, A., Linssen, A.B., and Berendsen, H.J. (1993). Essential dynamics of proteins. Proteins *17*, 412–425.

Avruch, J., Belham, C., Weng, Q., Hara, K., and Yonezawa, K. (2001). The p70 S6 kinase integrates nutrient and growth signals to control translational capacity. Prog. Mol. Subcell. Biol. *26*, 115–154.

Bain, J., McLauchlan, H., Elliott, M., and Cohen, P. (2003). The specificities of protein kinase inhibitors: an update. Biochem. J. *371*, 199–204.

Biondi, R.M., Cheung, P.C., Casamayor, A., Deak, M., Currie, R.A., and Alessi, D.R. (2000). Identification of a pocket in the PDK1 kinase domain that interacts with PIF and the C-terminal residues of PKA. EMBO J. *19*, 979–988.

Biondi, R.M., Komander, D., Thomas, C.C., Lizcano, J.M., Deak, M., Alessi, D.R., and van Aalten, D.M.F. (2002). High resolution crystal structure of the human PDK1 catalytic domain defines the regulatory phosphopeptide docking site. EMBO J. *21*, 4219–4228.

Brazil, D.P., and Hemmings, B.A. (2001). Ten years of protein kinase B signalling: a hard Akt to follow. Trends Biochem. Sci. *26*, 657–664.

Brunger, A.T., Adams, P.D., Clore, G.M., DeLano, W.L., Gros, P., Grosse-Kunstleve, R.W., Jiang, J.S., Kuszewski, J., Nilges, M., Pannu, N.S., et al. (1998). Crystallography & NMR system: a new software suite for macromolecular structure determination. Acta Crystallogr. D Biol. Crystallogr. *54*, 905–921.

Davis, P.D., Elliott, L.H., Harris, W., Hill, C.H., Hurst, S.A., Keech, E., Kumar, M.K., Lawton, G., Nixon, J.S., and Wilkinson, S.E. (1992a). Inhibitors of protein kinase C. 2. Substituted bisindolylmaleimides with improved potency and selectivity. J. Med. Chem. *35*, 994–1001.

Davis, P.D., Hill, C.H., Lawton, G., Nixon, J.S., Wilkinson, S.E., Hurst, S.A., Keech, E., and Turner, S.E. (1992b). Inhibitors of protein kinase C. 1. 2,3-Bisarylmaleimides. J. Med. Chem. *35*, 177–184.

Davies, S.P., Reddy, H., Caivano, M., and Cohen, P. (2000). Specificity and mechanism of action of some commonly used protein kinase inhibitors. Biochem. J. *351*, 95–105.

de Groot, B.L., Hayward, S., van Aalten, D.M., Amadei, A., and Berendsen, H.J. (1998). Domain motions in bacteriophage T4 lysozyme: a comparison between molecular dynamics and crystallographic data. Proteins *31*, 116–127.

Eyers, P.A., Craxton, M., Morrice, N., Cohen, P., and Goedert, M. (1998). Conversion of SB 203580-insensitive MAP kinase family members to drug-sensitive forms by a single amino-acid substitution. Chem. Biol. *5*, 321–328.

Eyers, P.A., van den IJssel, P., Quinlan, R.A., Goedert, M., and Cohen, P. (1999). Use of a drug-resistant mutant of stress-activated protein kinase 2a/p38 to validate the in vivo specificity of SB 203580. FEBS Lett. *451*, 191–196.

Fabre, S., Prudhomme, M., and Rapp, M. (1993). Protein kinase C inhibitors: structure-activity relationships in K252c-related compounds. Bioorg. Med. Chem. *1*, 193–196.

Faul, M.M., Winneroski, L.L., Krumrich, C.A., Sullivan, K.A., Gillig, J.R., Neel, D.A., Rito, C.J., and Jirousek, M.R. (1998). Macrocyclic bisindolylmaleimides: synthesis by inter- and intramolecular alkylation. J. Org. Chem. *63*, 1961–1973.

Frodin, M., and Gammeltoft, S. (1999). Role and regulation of 90 kDa ribosomal S6 kinase (RSK) in signal transduction. Mol. Cell. Endocrinol. *151*, 65–77.

Frodin, M., Jensen, C.J., Merienne, K., and Gammeltoft, S. (2000). A phosphoserine-regulated docking site in the protein kinase RSK2 that recruits and activates PDK1. EMBO J. *19*, 2924–2934.

Frodin, M., Antal, T.L., Dummler, B.A., Jensen, C.J., Deak, M., Gammeltoft, S., and Biondi, R.M. (2002). A phosphoserine/threonine-binding pocket in AGC kinases and PDK1 mediates activation by hydrophobic motif phosphorylation. EMBO J. *21*, 5396–5407.

Goekjian, P.G., and Jirousek, M.R. (1999). Protein kinase C in the treatment of disease: signal transduction pathways, inhibitors, and agents in development. Curr. Med. Chem. *6*, 877–903.

Hooft, R.W., Sander, C., and Vriend, G. (1996). Positioning hydrogen atoms by optimizing hydrogen-bond networks in protein structures. Proteins *26*, 363–376.

Hunenberger, P.H., Helms, V., Narayana, N., Taylor, S.S., and McCammon, J.A. (1999). Determinants of ligand binding to cAMP-dependent protein kinase. Biochemistry *38*, 2358–2366.

Jeffrey, P.D., Russo, A.A., Polyak, K., Gibbs, E., Hurwitz, J., Massague, J., and Pavletich, N.P. (1995). Mechanism of CDK activation revealed by the structure of a cyclinA-CDK2 complex. Nature *376*, 313–320.

Jirousek, M.R., Gillig, J.R., Neel, D.A., Rito, C.J., Obannon, D., Heath, W.F., McDonald, J.H., Faul, M.M., Winneroski, L.L., Melikianbadal-

ian, A., et al. (1995). Synthesis of bisindolylmaleimide macrocycles. Bioorg. Med. Chem. Lett. *5*, 2093–2096.

Jirousek, M.R., Gillig, J.R., Gonzalez, C.M., Heath, W.F., McDonald, J.H., 3rd, Neel, D.A., Rito, C.J., Singh, U., Stramm, L.E., Melikian-Badalian, A., et al. (1996). (S)-13-[(dimethylamino)methyl]-10,11,14, 15-tetrahydro-4,9:16, 21-dimetheno-1H, 13H-dibenzo[e,k]pyrrolo[3,4-h] [1,4,13]oxadiazacyclohexadecene-1,3(2H)-d ione (LY333531) and related analogues: isozyme selective inhibitors of protein kinase C beta. J. Med. Chem. *39*, 2664–2671.

Johnson, L.N., Noble, M.E., and Owen, D.J. (1996). Active and inactive protein kinases: structural basis for regulation. Cell *85*, 149–158.

Johnson, D.A., Akamine, P., Radzio-Andzelm, E., Madhusudan, M., and Taylor, S.S. (2001). Dynamics of cAMP-dependent protein kinase. Chem. Rev. *101*, 2243–2270.

Jones, T.A., Zou, J.Y., Cowan, S.W., and Kjeldgaard (1991). Improved methods for building protein models in electron density maps and the location of errors in these models. Acta Crystallogr. A *47 (Pt 2)*, 110–119.

Komander, D., Kular, G.S., Bain, J., Elliott, M., Alessi, D.R., and Van Aalten, D.M. (2003). Structural basis for UCN-01 (7-hydroxystaurosporine) specificity and PDK1 (3-phosphoinositide-dependent protein kinase-1) inhibition. Biochem. J. *375*, 255–262.

Lang, F., and Cohen, P. (2001). Regulation and physiological roles of serum- and glucocorticoid-induced protein kinase isoforms. Sci STKE *2001*, RE17.

Leslie, N.R., Biondi, R.M., and Alessi, D.R. (2001). Phosphoinositide-regulated kinases and phosphoinositide phosphatases. Chem. Rev. *101*, 2365–2380.

Morris, G.M., Goodsell, D.S., Halliday, R.S., Huey, R., Hart, W.E., Belew, R.K., and Olson, A.J. (1998). Automated docking using a Lamarckian genetic algorithm and an empirical binding free energy function. J. Comput. Chem. *19*, 1639–1662.

Murshudov, G.N., Vagin, A.A., and Dodson, E.J. (1997). Refinement of macromolecular structures by the maximum- likelihood method. Acta Crystallogr. D Biol. Crystallogr. *53*, 240–255.

Nakamura, J., Kato, K., Hamada, Y., Nakayama, M., Chaya, S., Nakashima, E., Naruse, K., Kasuya, Y., Mizubayashi, R., Miwa, K., et al. (1999). A protein kinase C-beta-selective inhibitor ameliorates neural dysfunction in streptozotocin-induced diabetic rats. Diabetes *48*, 2090–2095.

Narayana, N., Diller, T.C., Koide, K., Bunnage, M.E., Nicolaou, K.C., Brunton, L.L., Xuong, N.H., Ten Eyck, L.F., and Taylor, S.S. (1999). Crystal structure of the potent natural product inhibitor balanol in complex with the catalytic subunit of cAMP-dependent protein kinase. Biochemistry *38*, 2367–2376.

Navaza, J. (2001). Implementation of molecular replacement in AMoRe. Acta Crystallogr. D Biol. Crystallogr. *57*, 1367–1372.

Newton, A.C. (2001). Protein kinase C: structural and spatial regulation by phosphorylation, cofactors, and macromolecular interactions. Chem. Rev. *101*, 2353–2364.

Newton, A.C. (2003). Regulation of the ABC kinases by phosphorylation: protein kinase C as a paradigm. Biochem. J. *370*, 361–371.

Ohtsuka, T., and Zhou, T. (2002). Bisindolylmaleimide VIII enhances DR5-mediated apoptosis through the MKK4/JNK/p38 kinase and the mitochondrial pathways. J. Biol. Chem. *277*, 29294–29303.

Otwinowski, Z., and Minor, W. (1997). Processing of X-ray diffraction data collected in oscillation mode. Methods Enzymol. *276*, 307–326.

Prade, L., Engh, R.A., Girod, A., Kinzel, V., Huber, R., and Bossemeyer, D. (1997). Staurosporine-induced conformational changes of cAMP-dependent protein kinase catalytic subunit explain inhibitory potential. Structure *5*, 1627–1637.

Scheid, M.P., and Woodgett, J.R. (2001). PKB/AKT: functional insights from genetic models. Nat. Rev. Mol. Cell Biol. *2*, 760–768.

Takahashi, I., Kobayashi, E., Asano, K., Yoshida, M., and Nakano, H. (1987). Ucn-01, a selective inhibitor of protein-kinase-C from Streptomyces. J. Antibiot. (Tokyo) *40*, 1782–1784.

Toullec, D., Pianetti, P., Coste, H., Bellevergue, P., Grand-Perret, T., Ajakane, M., Baudet, V., Boissin, P., Boursier, E., Loriolle, F., et al. (1991). The bisindolylmaleimide GF 109203X is a potent and selective inhibitor of protein kinase C. J. Biol. Chem. *266*, 15771–15781.

van Aalten, D.M.F., Bywater, R., Findlay, J.B., Hendlich, M., Hooft, R.W., and Vriend, G. (1996). PRODRG, a program for generating molecular topologies and unique molecular descriptors from coordinates of small molecules. J. Comput. Aided Mol. Des. *10*, 255–262.

van Aalten, D.M., Conn, D.A., de Groot, B.L., Berendsen, H.J., Findlay, J.B., and Amadei, A. (1997). Protein dynamics derived from clusters of crystal structures. Biophys. J. *73*, 2891–2896.

van Aalten, D.M., Chong, C.R., and Joshua-Tor, L. (2000). Crystal structure of carboxypeptidase A complexed with D-cysteine at 1.75 A: inhibitor-induced conformational changes. Biochemistry *39*, 10082–10089.

Vlahos, C.J., McDowell, S.A., and Clerk, A. (2003). Kinases as therapeutic targets for heart failure. Nat. Rev. Drug Discov. *2*, 99–113.

Volarevic, S., and Thomas, G. (2001). Role of S6 phosphorylation and S6 kinase in cell growth. Prog. Nucleic Acid Res. Mol. Biol. *65*, 101–127.

Vriend, G. (1990). WHAT IF: a molecular modeling and drug design program. J. Mol. Graph. *8*, 52–56, 29.

Xie, G.J., and Lown, J.W. (1994). A facile synthesis of staurosporine aglycone. Tetrahedron Lett. *35*, 5555–5558.

Zhou, T., Song, L., Yang, P., Wang, Z., Lui, D., and Jope, R.S. (1999). Bisindolylmaleimide VIII facilitates Fas-mediated apoptosis and inhibits T cell-mediated autoimmune diseases. Nat. Med. *5*, 42–48.

Zhao, B., Bower, M.J., McDevitt, P.J., Zhao, H., Davis, S.T., Johanson, K.O., Green, S.M., Concha, N.O., and Zhou, B.B. (2002). Structural basis for Chk1 inhibition by UCN-01. J. Biol. Chem. *277*, 46609–46615.

Accession Numbers

The coordinates and structure factors have been deposited with the PDB (entries PDK1-LY333531: 1uu3, PDK1-BIM1: 1uu8, PDK1-BIM2: 1uu7, PDK1-BIM3: 1uu9, and PDK1-BIM8: 1uvr).